PCCP

Accepted Manuscript

ROYAL SOCIETY OF CHEMISTRY

www.rsc.org/pccp

Local Photo-Oxidation of Individual Single Walled Carbon Nanotubes Probed by Femtosecond Four Wave Mixing Imaging

*Jukka Aumanen[1], Andreas Johansson[2], Olli Herranen[2], Pasi Myllyperkiö[1], Mika Pettersson[1,]**

Nanoscience Center, Departments of Chemistry[1] and Physics[2], P.O. Box 35, FI-40014, University of Jyväskylä, Finland

ABSTRACT. Photo-oxidation of individual, air-suspended single walled carbon nanotubes (SWCNT) is studied by femtosecond laser spectroscopy and imaging. Individual SWCNTs are imaged by four wave mixing (FWM) microscopy under inert gas (Ar, N_2) atmosphere. When imaging is performed in ambient air atmosphere, decay of the FWM signal takes place. Electron microscopy shows that SWCNTs are not destroyed and the process is attributed to photoinduced oxidation reactions which proceed via non-linear excitation mechanism, when irradiation is performed with ~30 fs pulses in the visible spectral region (500 – 600 nm). Photo-oxidation can be localized in specific regions of SWCNTs within optical resolution (~300 nm). The effect of photo-oxidation on Raman spectra was studied by irradiating a local spot on an individual SWCNT and comparing spectra of irradiated and non-irradiated regions of the same tube. It is shown at an individual nanotube level that oxidation leads to decrease of intensity of Raman signal and an upshift of the G-band.

Keywords: Carbon nanotube, oxidation, four wave mixing, imaging, multiphoton, spectroscopy

Introduction

Due to their exceptional electronic and optical properties, Carbon nanotubes (CNT) are promising building blocks for many applications. However, despite the huge research effort directed towards them over the last few decades, many challenges remain before advanced applications become commonplace. Significant obstacle for broader use of SWCNTs in applications is the current lack of methods to produce in large scale nanotubes with specific chiral indices (n,m). Substantial research effort has been directed for development of purification methods for separating different tube types from an ensemble[1-3] and for development of synthesis methods for producing narrow distribution of SWCNTs.[4] While important progress has been made in these areas we are still far from being able to produce pure materials with desired properties.

Development of ultra-small scale electronics is a major driving force for carbon nanotube research. Despite the problems with synthesis, important steps are being taken in this direction as was shown recently by the development of a CNT computer.[5] A particular problem for development of CNT based electronics is the presence of metallic nanotubes in an ensemble of semiconducting nanotubes. To overcome this problem, techniques for separating metallic and semiconducting nanotubes have been developed.[6] An alternative strategy is to convert metallic nanotubes to semiconducting by various methods. Oxidation of CNTs by UV light in the presence of oxygen has been observed.[7,8] Oxidation of CNTs by ozone leads to increase of their electrical resistance.[9] This effect was exploited in a development of a scalable method for metal to semiconductor conversion of CNTs for electric device applications.[10] Further developments have concentrated on patterning of CNT thin films exploiting oxidation.[11,12] As a result of these

studies, (photo) oxidation of CNTs has turned out to be a useful process for development of technologies for CNT based electronic devices.

Non-linear optical processes are prominent in CNTs but so far they have been much less studied than linear processes. Sheps et al. used four wave mixing (FWM) microscopy for imaging of SWCNTs on surfaces.[13] Myllyperkiö et al. performed FWM measurements of individual air-suspended SWCNTs with time resolved (femtosecond) methods.[14] Second harmonic generation (SHG) was observed for SWCNT ensembles indicating very large second order susceptibilities, in agreement with electronic structure calculations.[15,16] Very strong intrinsic SHG response was confirmed by observing SHG from an individual air-suspended SWCNT.[17]

It has been observed by using emission spectroscopy that interaction of oxygen with individual SWCNTs may lead to blinking or bleaching of luminescence, activation of forbidden transitions and creation of new states.[18–21] While luminescence studies are limited to semiconducting SWCNTs, FWM spectroscopy is sensitive to metallic tubes as well which makes FWM a more general method for investigating SWCNTs. FWM microscopic studies of CNTs lying on surfaces revealed that liquid phase electrochemical oxidation leads to degradation of the FWM signal due to covalent sidewall reactions.[13]

In this paper, we study laser-induced oxidation of suspended individual SWCNTs with femtosecond FWM imaging. Experimental arrangement for FWM imaging allows simultaneous controlled local photo-oxidation of SWCNTs and their imaging with high sensitivity. Photo-oxidation of SWCNTs occurs via non-linear processes in the visible wavelength range (500 – 600 nm). Raman measurements on oxidized and non-oxidized areas of the same individual suspended nanotube establish that oxidation correlates with decrease of the FWM and Raman

signals and up-shift of the G-band frequency. The results are important for development of laser-based modification, imaging and analysis methods for SWCNTs.

Experimental

Sample Fabrication. A Si chip with LPCVD (low pressure chemical vapor deposition) grown Si_3N_4 film (300 nm thick) was used as starting material. A membrane window was then fabricated with standard lithography processes containing e-beam patterning, plasma etching and wet etching. As a final step, a narrow slit was etched in the membrane window (2-3 μm wide), with another e-beam lithography round.

Nanotubes were then grown across the slit by using alcohol-CVD.[22] An iron (Fe) thin film (~1 nm) was evaporated as a catalyst layer by patterning small islands of it in close vicinity of the slits. The samples were then loaded to a preheated (T = 850 °C) tube furnace via a loadlock system. A 20 minute reduction step was done in constant Ar/H_2 (6 % of Hydrogen) mixture with ca. 200 sccm flow rate. The Ar/H_2 gas mixture was then bubbled through ice-chilled ethanol for 20 minutes to grow the tubes. Then the samples were unloaded under Ar/H_2 flow

Scanning Electron Microscopy. The locations of the CNTs grown across the slit were mapped by imaging, using a Raith e-line SEM (scanning electron microscope). The images were taken using 10 kV acceleration voltage and around 2000-5000 magnification which provided good conditions to observe individual CNTs. Typical area dose was kept as low as possible (<900 $\mu As/cm^2$) to minimize the contamination of the tubes caused by the e-beam.[23] The tubes were imaged again after the FWM experiments to check that the tubes were still intact and lying at the original positions.

Transmission Electron Microscopy. The individual CNTs were imaged with a JEOL JEM-1400 transmission electron microscope, using minimal exposure time and acceleration voltage of at most 80 kV acceleration voltage to avoid beam induced damage. The impinging electrons thus carry significantly less energy than the about 100 keV required for knock-on removal of carbon atoms from the CNT.[24]

FWM Imaging. A home-built femtosecond FWM microscope system, shown schematically in Fig. 1, contains a high repetition rate amplified fs-laser system and microscope. The amplified fs-laser (Pharos-10, 600 kHz, Light Conversion) pumps two non-collinear parametric amplifiers (NOPAs, Orpheus-N, Light Conversion). Both NOPAs can be tuned individually from 510 nm to 890 nm, allowing two color CARS frequency to be tuned between 0-3000 cm^{-1}. NOPAs are tuned to produce ~30 fs pulses over the visible region. Optical setup contains additional prism compressors (fused silica prisms) for compensating additional glass in the microscope setup. Relative time delays between all three pulses can be tuned by computer controlled optical delay lines (Thorlabs). Three beams are combined using beam splitters, and directed to the microscope objective in collinear geometry.

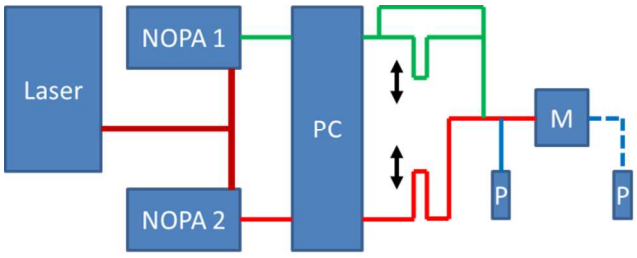

Fig. 1 Optical arrangement for two-color Four Wave Mixing Microscopy. PC = pulse compressors, P = Photon Counting Avalanche Photodiode, M = Microscope.

The microscope contains home-built microscope body, high NA microscope objective (Nikon LU Plan ELWD 100x/0.80), a tube lens, signal detection and a camera for viewing the sample.

Signal detection is based on photon counting scheme (single photon avalanche photodiode, SPCM-AQRH-14, Excelitas Technologies). Residuals of the laser radiation are removed using a dichroic long pass filters (Semrock) and a detection wavelength is selected using a band pass filter (Semrock). Detection can be done in either forward or backscattering directions. Sample is placed on piezo-stages (Thorlabs) and imaging is performed with a point scan method. Typical detection time is 0.2-0.4 s/point. Typical time resolution for the microscope system is around 40 fs. The spatial resolution is on the order of 300 nm. Pulse energies were typically less than 12 pJ.

Raman Microscopy. Raman measurements were performed with a home-built Raman spectrometer/microscope equipped with a frequency-doubled single mode laser (Alphalas, MONOPOWER-532-100-SM), edge filter (Semrock), imaging spectrograph (Acton Research Corporation, SpectraPro 2500i) and a cooled CCD camera (Andor Technologies, Newton). The excitation wavelength was 532 nm, excitation power was 2 mW, and the measurement time was 10 s. The used grating had 600 lines/mm yielding a practical resolution of ~10 cm^{-1}. For microspectroscopy, the laser beam was focused to the sample with a microscope objective Nikon L Plan SLWD 100x/0.70 and the sample was visualized with a CCD based web camera. Illumination was performed with a ring light equipped with a set of white LEDs. The sample was moved with a piezo X-Y-Z stage (Thorlabs NanoMax 300) allowing accurate movement with a spatial resolution of 5 nm.

Results

FWM Imaging. SWCNTs suspended over slits were imaged with femtosecond FWM which is a sensitive method for studying individual SWCNTs.[13,14,25] FWM signal is substantially

enhanced when at least one of the excitation beams is in electronic or vibrational resonance with SWCNT.[25] Therefore the difference in the energy of pump and Stokes frequencies was tuned to match the Raman transition of the G-band (1590 cm^{-1}). It should be noted, however, that in SWCNTs electronic resonance enhancement overwhelms vibrational resonances and thus imaging is not practically sensitive to the actual Stokes shift but more important factor is the electronic resonance of the tubes.[25]

Initial attempts to observe signal from SWCNTs failed until it was realized that laser irradiation of SWCNTs in ambient air led to rapid decay of signal. To overcome this problem, the sample was mounted in a chamber, which was purged with argon or nitrogen gas. This allowed the samples to be imaged without significant decay of signal. Purging with several gases was tested and it was found that signal bleaching required presence of oxygen, identifying the process(es) responsible for signal bleaching as photo-induced oxidation. Typically 2 L/min gas flow was enough to prevent bleaching of the FWM signal. Nevertheless there is some variation in oxidation rate between different SWCNTs and some of them seem to be more resistant to bleaching than others. Various pulse energies were tested for imaging and it was found that good signals were obtained at very low pulse energies of ~10 pJ for both laser beams, corresponding to time-integrated total power of ~12 μW at 600 kHz. Notice that this is about two orders of magnitude lower than what is typically used in Raman imaging of SWCNTs, demonstrating the great sensitivity of FWM for SWCNTs.[13,14,25,26]

Mapping FWM signal over the area of a slit reveals the locations of the suspended SWCNTs, but the strength of the FWM signal varies considerably from tube to tube. Those SWCNTs that are in electronic resonance with either of the excitation frequencies give relatively strong FWM response while off-resonant SWCNTs are hardly distinguishable from the background. A typical

FWM slit image is illustrated in Fig. 2 (left panel) with the corresponding SEM image (right panel).

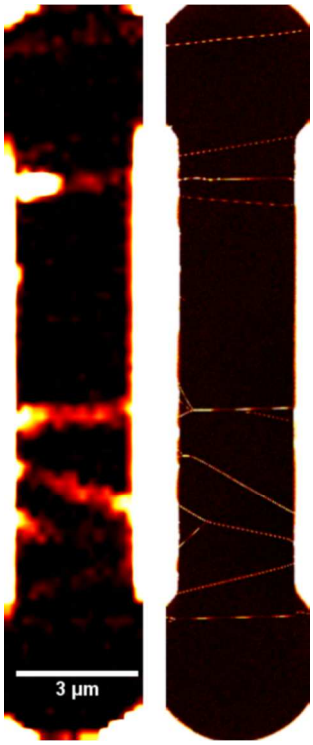

Fig 2 FWM (left) and SEM (right) images of SWCNTs hanging over a slit.

FWM image in Fig. 2 was measured using excitation pulses with center wavelengths of 590 nm (pump) and 650 nm (Stokes) and pulse energies of 8 pJ. The sample was moved in 0.2 µm steps and collecting signal 0.2 seconds at each point. The overall time to image the slit took five minutes.

Individual SWCNTs can be imaged more precisely by increasing the signal collection time and shortening the imaging step size. SWCNT, being much smaller in diameter than the focal spot, allows also quantification of the size of the focus, establishing spatial resolution of the FWM imaging method. Fig. 3 presents an image of a single SWCNT (or a small bundle) measured with one second collection time per pixel and 0.1 µm pixel spacing, while other parameters are the

same as in the image in Fig. 2. Increased resolution and collection time extend total measuring time of the map to 18 minutes. Under nitrogen purging, the sample is stable in this time scale. The cross-section of the nanotube is presented in the inset to establish the optical resolution of the measurement as 300 nm (FWHM).

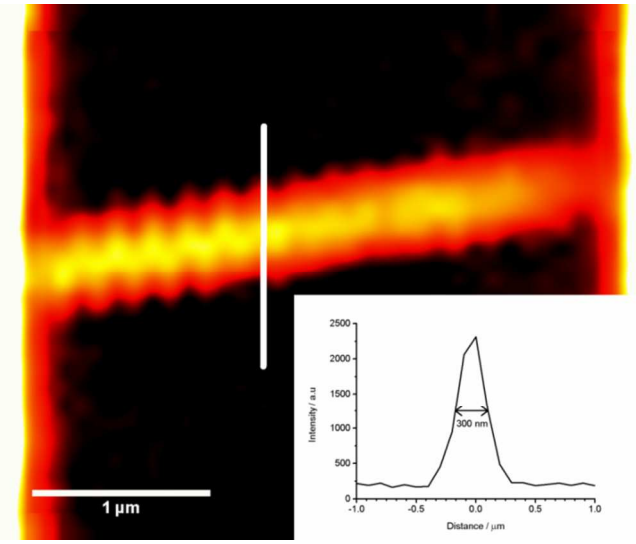

Fig. 3 FWM image of a SWCNT crossing a slit. The inset shows the cross-section of the SWCNT along the line marked in the figure.

The FWM signal is dependent on laser polarization and the strongest signal is observed when polarization of the excitation beam is parallel with the long axis of the SWCNT.[25] We tested polarization dependence with a loop sample, shown in Fig. 4. Panel A shows the image obtained with vertical polarization (with respect to the image axes) showing only the section of the loop that is oriented parallel with the polarization direction. Rotating the polarization to horizontal direction yields the image in panel B, showing only the sections of the tube which are parallel with horizontal polarization. A TEM image of the looped SWCNT is presented in Fig. 4(C).

Panel D shows FWM intensity profile along the white line in Fig. 4(B) to demonstrate the contrast that is achieved with the polarization.

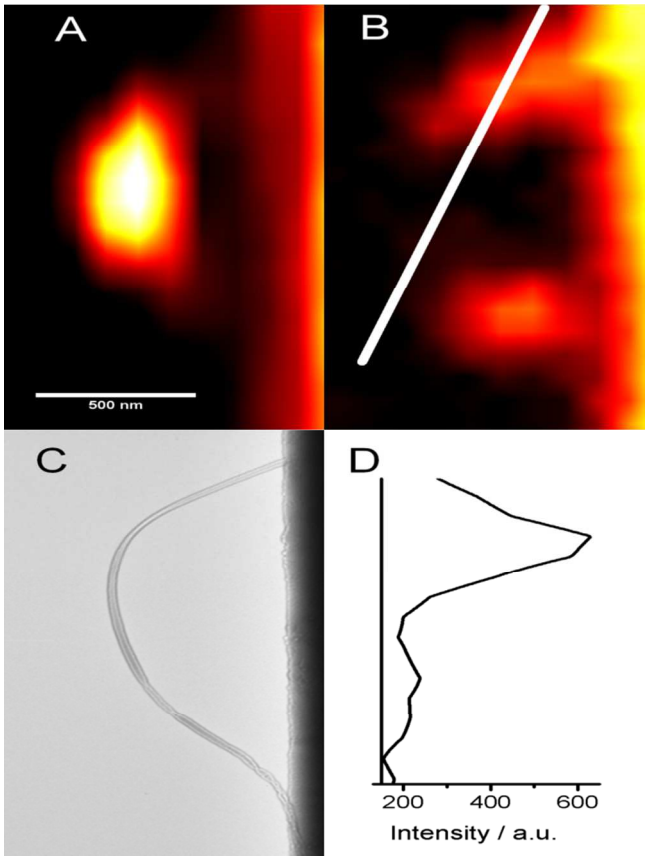

Fig. 4 FWM images of a loop sample of SWCNT with (A) vertical and (B) horizontal polarizations of excitation beams. (C) Corresponding TEM image. (D) Intensity profile along the line marked in Fig. 4(B) with horizontal polarization.

While imaging of the nanotubes can be performed over extended time without a noticeable drop in signal levels under nitrogen or argon purging, once the purge is switched off the signal decreases rapidly. A typical decay of signal is shown in Fig. 5. Initially the sample chamber was purged with an argon flow, which was then switched off during measurement as indicated in the Figure.

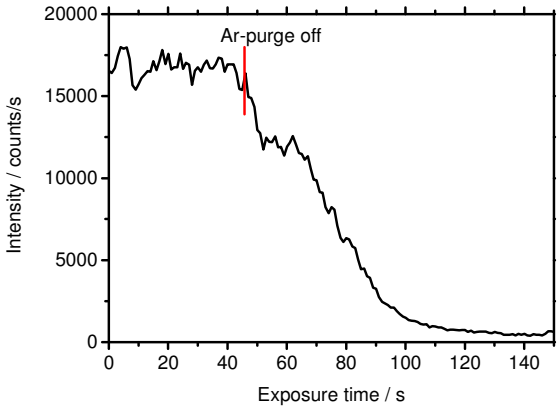

Fig. 5 FWM signal measured from a SWCNT under argon flow that is switched off during measurement. Pump and Stokes pulse energies at the sample were 8 pJ and repetition rate was 600 kHz.

Decay of the FWM signal is local and irreversible. Bleaching is restricted to the spot where the laser beams are focused, but the rest of the nanotube is unaffected. The locality of bleaching is demonstrated in Fig. 6 in which images before (Fig. 6A) and after (Fig. 6B) local irradiation show dark areas restricted to the irradiated spots. Thus, it is possible to localize the oxidation in SWCNTs approximately with optical spatial resolution (~300 nm). The decay signal presented in Fig. 5 was measured from the lower nanotube of Figure 6 between taking the images 6(A) and 6(B). Laser beams (pump 590 nm, Stokes 650 nm) were kept focused to a single spot and argon purge was switched off and SWCNTs were irradiated three minutes before the beams were blocked. After that argon purge was switched on again and the FWM imaging was repeated.

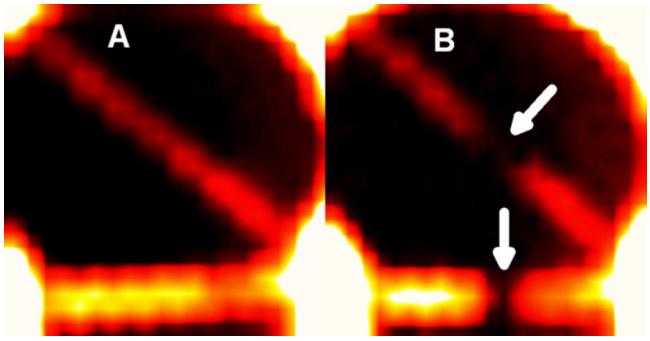

Fig. 6 (A) FWM image of two SWCNTs over a slit. (B) Same SWCNTs after irradiation of the selected spots without purging with argon. The two spots were irradiated with two laser beams at 590 and 650 nm each having 5 μW power (8 pJ pulse energy) at the sample with 600 kHz repetition rate.

Although FWM signal is locally and permanently lost, TEM images (not shown) do not show any noticeable structural changes in SWCNTs. They are still unbroken and the bleached part cannot be distinguished from the rest of the tube in the TEM images. Nonetheless when pulse energies are significantly increased to tens of pJ, SWCNTs were sometimes observed to brake or detach from the slit regardless of purging.

In order to study the mechanism of photo-oxidation in more detail, dependence of the rate of bleaching of the FWM signal on excitation pulse energy was studied. In order to overcome the problems associated with variation of the bleach rate from tube to tube and with accurate alignment of the focus in different areas of the sample, individual SWCNTs were studied. One SWCNT was chosen and the laser was focused on a specific part of the tube. Purge was stopped after which the kinetics of signal decay was measured. Then the purge was put on again and the laser beam having different pulse energy was focused to another spot of the same tube. In these studies the Stokes energy was kept constant (6 pJ/pulse) and the pump pulse energy was varied from 3 pJ to 6 pJ. These measurements are extremely difficult since they require utmost stability

during the measurement. Results for one representative case are plotted in Fig. 7, showing signal decay at two different pulse energies for the same tube. The dependence of the decay rate on pulse energy is non-linear, as deduced from exponential fits. The ratio of the decay constants in this particular case is 8.3 while the ratio of pulse energies is 2. Assuming multiphoton process the order is close to three-photon dependence, which should give a ratio of 8. For other tubes the dependence varied but it was always higher than linear, establishing that photo-oxidation is a nonlinear process in our conditions. More accurate determination of the power-dependence would require improving the stability of the setup. It is important to note that oxidation could be induced by either pump or Stokes pulse depending on the tube. Sometimes oxidation was insensitive to either pump or Stokes while sometimes it depended on both. This shows that oxidation depends on electronic resonance of the tube and thus requires direct excitation of SWCNT.

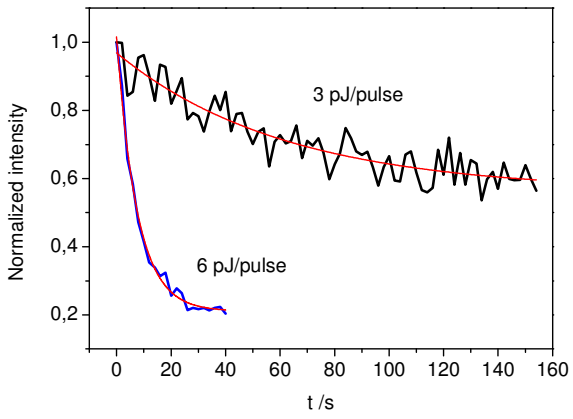

Fig. 7. Photoinduced decay of the FWM signal measured from an individual SWCNT in air atmosphere. The Stokes pulse energy was 6 pJ and Pump pulse energy was varied from 3 pJ (black curve) to 6 pJ (blue curve). The red curves show single-exponential fits to the data.

Raman Microspectroscopy. Local photo-oxidation was additionally studied by Raman microspectroscopy. Again, an individual tube (or small bundle) was chosen which was resonant with the Raman laser (532 nm). The FWM pump laser, which was used for excitation, was tuned to the same wavelength (532 nm) ensuring that photo-oxidation was induced resonantly in the same tube that was probed by Raman spectroscopy. This is important in order to exclude the possibility that in a small bundle one tube is photo-oxidized but another tube is probed in Raman due to different resonance conditions. After checking that the tube is resonant with the Raman laser, FWM image was recorded which was followed by photo-oxidation of a local spot. Then Raman spectra were measured along the tube in several spots by moving the laser focus step by step in x-direction and optimizing the signal at every step in y- and z-directions. Representative Raman spectra are shown in Fig. 8 and the data extracted from Raman spectra is presented in Fig. 9 together with FWM image.

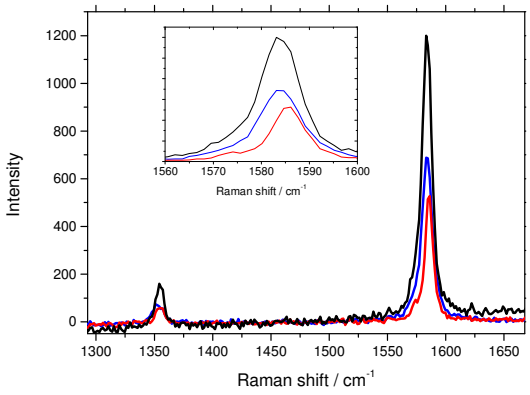

Fig. 8 Raman spectra of an air-suspended partially oxidized individual SWCNT. The spectra are measured at different positions of the SWCNT: black spectrum is measured from unoxidized region of SWCNT while red and blue spectra are measured from partially oxidized regions.

Raman spectra in Fig. 8 are measured from unoxidized (black) and partially oxidized (red, blue) regions of SWCNT. It can be seen that the intensity of the peaks decreases in oxidized regions compared to spectrum from unoxidized region and, additionally, the G-band shifts up in oxidized regions.

In Fig. 9, Raman data are shown as a function of position on the SWCNT. Three important characteristics are evident. First, the G-band intensity, or area, shows clearly that intensity decreases locally in the oxidized area. The drop in intensity is a factor of about three compared to the right side of the tube and slightly more than a factor of two compared to the left side of the tube. Second, the intensity of the D-band also decreases locally due to oxidation and the trend follows closely the trend of the G-band. Accordingly, the ratio of the intensities of the G- and D-bands does not change significantly upon oxidation. Third, there is a clear local upshift of the G-band frequency upon oxidation. Although there is some variation observed along the tube, possibly induced by surface interactions, there is clear correlation of the G-band frequency shift locally in the oxidized area, the shift being +1.5 – +2.0 cm^{-1}.

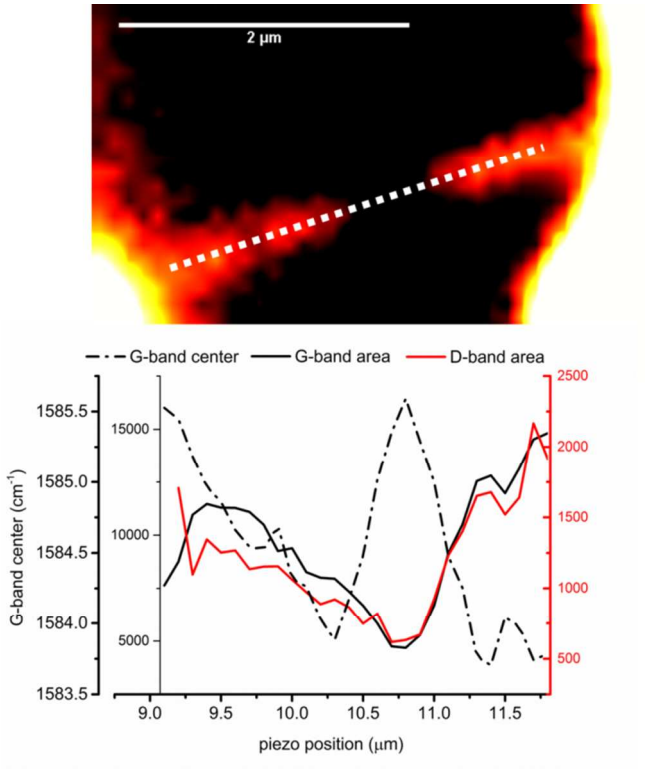

Fig. 9. FWM image (upper panel) and Raman data along the tube (lower panel) of a SWCNT suspended over a slit. The Raman data is acquired with a 0.1 µm step size. Photo-oxidation was locally induced in the tube by 532 nm excitation. In the lower panel G-band area is represented by a solid black line, D-band area by a solid red line, and G-band center by a black dash – dot line.

Discussion

Imaging. In Figs. 2 – 4, it is established that femtosecond FWM is a sensitive method for imaging of all kinds of SWCNTs. Previously, frequency domain (picosecond) FWM was used for imaging of CNTs on surfaces.[13,25] While in previous work mainly multiwalled carbon nanotubes (MWCNT) and metallic SWCNTs were studied because the signal levels from semiconducting SWCNTs were very weak, the present results show that for suspended tubes

signal levels are very good for all kinds of tubes, including individual semiconducting SWCNTs. It is notable that our average power level (~12 μW) is about three orders of magnitude lower than in a previous study of CNTs on a substrate,[13] showing the benefit of working with air-suspended samples which minimizes the background signal. Although we don't specifically characterize each SWCNT separately, we have obtained images of numerous SWCNTs and there is a good reason to believe that they include mostly semiconducting tubes and also some of them are individual. In our earlier work we established by electron diffraction that FWM signal was obtained from individual semiconducting tubes.[14] As noted earlier, the average power used at the level of tens of microwatts or less indicates very strong non-linear third order response of SWCNTs. The key to successful imaging of SWCNTs is elimination of photoinduced oxidation by purging. Alternatively, vacuum conditions could be used but it requires more complex technical solution. The variation of signal levels for different tubes in Fig. 2 most probably originate from different resonance conditions and from different thickness of the tubes.[13] Fig. 3 establishes the practical optical resolution to be ~300 nm which potentially could be further improved by using higher numerical aperture objective.

Photo-oxidation. There is a good reason to believe that the process leading to decrease of the FWM signal is oxidation. The fact that oxygen is required for the process already strongly points to this interpretation. Sheps et al. studied electrochemical oxidation of CNTs in liquid phase and they showed that sidewall functionalization leads to decay of FWM signal.[13] Previously, photoinduced oxidation by O_2 has been observed and studied for ensemble CNT samples[7,8] and for individual SWCNTs.[18-21] XPS and computational studies have shown that plausible interpretation for the microscopic mechanism of oxidation is covalent attachment of oxygen to the carbon nanotube sidewalls as carbonyl, epoxy and hydroxyl groups.[8,27] Additional IR-

spectroscopic evidence supports this picture.[8] The mechanism of oxidation in our case involves multiphoton excitation, as shown in Fig. 7. This indicates that the energy of single photon is not sufficient for oxidation, which is in line with previous studies where linear photo-oxidation of SWCNTs was induced with UV-radiation in the 200 – 400 nm region.[7,8]

There are several possibilities for the mechanism of oxidation. In principle, heating of SWCNT to above 730 °**C** could lead to oxidation as estimated from burning temperatures of SWCNTs determined by thermogravimetry.[28] We disregard this mechanism since the used average power is way too low to lead to any significant heating of the tubes. Typically average powers in the mW range are used in tight focusing conditions for heating of suspended SWCNTs as observed by Raman spectroscopy.[29,30] Naturally for a very short time after excitation the temperature of the tube can rise due to conversion of electronic excitation to heat via various dissipation mechanisms. Excited electrons lose their energy to phonons via electron phonon scattering which occurs in a subpicosecond timescale.[31] Classical molecular dynamics simulation show that heat conduction from the area heated by an ultrafast heat pulse occurs in a picosecond timescale in SWCNTs.[32] Thus, we can expect that the excited area remains hot during few picoseconds after the excitation pulse which is not favorable for thermal reaction. We can estimate the maximal temperature jump by assuming excitation of one exciton with a length of 3 nm for a nanotube with a diameter of 2 nm. This model system contains about 720 atoms. Using the heat capacity of graphite of 700 J $kg^{-1}K^{-1}$ and a photon wavelength of 530 nm the maximal temperature rise is ~39 K. Thus, we can safely exclude thermal reaction. Finally, the multiphoton nature of photo-oxidation indicates non-thermal reaction since linear absorption should be the dominant mechanism of heating of the tube.

Oxidation of SWCNTs has been achieved previously by using reaction with ozone at elevated temperatures.[12] One possible mechanism for oxidation would involve production of either ozone or singlet oxygen in the gas phase which subsequently reacts with the walls of SWCNT as singlet oxygen is known to be more reactive with SWCNTs than triplet oxygen.[33] However, this mechanism is not compatible with the local character of oxidation following approximately the size of the focal spot. Thus, we believe that SWCNT is directly involved in the excitation process as is also indicated by the dependence of oxidation rate on resonance condition of SWCNTs.

Raman Microspectroscopy. The combination of individual, suspended nanotube samples and locality of photo-oxidation gives an opportunity to investigate the effect of oxidation on the Raman spectrum at a single tube level without any perturbing interactions with substrates or other nanotubes. Previously, there have been reports of upshift of the G-band by several wave numbers upon oxidation of SWCNT ensembles in liquid phase.[34] Evidence from XPS measurements establish that there are several chemical groups resulting from oxidation including C=O, C-O-C, and OH-groups.[8,9,27] Physisorption leads to only weakly bound oxygen species which presumably cannot induce significant changes in the Raman spectra.[35] Guo et al. studied computationally the effect of oxidation on the Raman spectra using a model of cycloaddition (-C-O-O-C-) on a (10,0) SWCNT.[36] They found that the G-band upshifts and then downshifts depending on the degree of coverage. In their model our observed upshift of 1.5 – 2 cm^{-1} would correspond to O/C ratio of about 0.01, i.e. 1 %, which seems reasonable. Additionally, Guo et al. observed that oxidation has a significant effect on the electronic structure of SWCNT.[36] Already at an O/C ratio of 0.05 the optical absorption spectrum of (10,0) tube is strongly modified. This finding can qualitatively explain the decrease of the FWM and Raman signal of SWCNTs upon oxidation. Thus, the changes in electronic structure lead to loss of electronic resonance

enhancement both in FWM and Raman, making them sensitive probes for oxidation. Loss of electronic resonance could be exploited as a mechanism of self-termination of oxidation, leading to uniform coverage and state of oxidation. This could be important in controlled laser writing of oxidized structures, which is a potential application of local photo-oxidation. Additionally, changes in chemical bonds upon oxidation change the nature of the Raman modes and their force constants, making the position of the G-band a sensitive probe for oxidation. There is one more observation from Fig. 9 that the D-band intensity decreases approximately at the same rate as the G-band upon oxidation, thus their ratio remains approximately the same. The ratio between the D- and G-bands is usually considered a good indicator for chemical functionalization but this study shows that it is not always the case as the resonance enhancement decreases due to functionalization and both G- and the D-bands lose their intensity simultaneously.[37]

Conclusions

Photo-oxidation of suspended SWCNTs with laser excitation was studied by femtosecond FWM imaging and Raman microspectroscopy. Photo-oxidation occurs via nonlinear excitation mechanism and it depends on electronic resonance of SWCNT. The presented experimental arrangement allows simultaneous oxidation and imaging of SWCNTs. Oxidation could be localized on a SWCNT approximately within optical resolution (~300 nm) forming a basis for laser based writing of oxidized structures on SWCNT based materials. Raman studies of an individual tube revealed an upshift by 1.5 – 2.0 cm^{-1} of the G-band upon oxidation. FWM and Raman signals decreased along with oxidation and this effect can be explained by the changes in the electronic structure of SWCNT leading to loss of the resonance with the laser.

AUTHOR INFORMATION

Corresponding Author

*Email: mika.j.pettersson@jyu.fi

Author Contributions

The manuscript was written through contributions of all authors. All authors have given approval to the final version of the manuscript.

Acknowledgements

This research was supported by the Academy of Finland (Decision no. 252468). O.H. was supported by personal grants from Jenny and Antti Wihuri Foundation and Finnish Cultural Foundation.

REFERENCES

1 X. Tu, S. Manohar, A. Jagota and M. Zheng, *Nature,* 2009, **460**, 250.

2 H. Liu, T. Tanaka, Y. Urabe and H. Kataura, *Nano Letters* 2013, **13**, 1996.

3 M. S. Arnold, A. A. Green, J. F. Hulvat, S. I. Stupp and M. C. Hersam, *Nat. Nanotechnol.* 2006, **1**, 60.

4 S. M. Bachilo, L. Balzano, J. E. Herrera, F. Pompeo, D. E. Resasco and R. B. Weisman, *J. Am. Chem. Soc.* 2003, **125**, 11186.

5 M. M. Shulaker, G. Hills, N. Patil, H. Wei, H.-Y. Chen, H.-S. P. Wong and S. Mitra, *Nature*, 2013, **501**, 526.

6 R. Krupke, F. Hennrich, H. v. Löhneysen and M.M Kappes, *Science*, 2003, **301**, 344.

7 T. Savage, S. Bhattacharya, B. Sadanadan, J. Gaillard, T. M. Tritt, Y.-P. Sun, Y. Wu, S. Nayak, R. Car, N. Marzari, P. M. Ayayan and A. M. J. Rao, *J. Phys. Condens. Matter*, 2000, **15**, 5195.

8 M. Lebrón-Colón, M. A. Meador, D. Luckzo, F. Solá, J. Santos-Pérez and L. S. McCorkle, *Nanotechnol.,* 2011, **22**, 455707.

9 J. M. Simmons, B. M. Nichols, S. E. Baker, M. S. Marcus, O. M. Castellini, C.-S. Lee, R. J. Hamers and M. A. Eriksson, *J. Phys. Chem. B,* 2006**, 110***,* 7113.

10 L. M. Gomez, A. Kumar, Y. Zhang, K. Ryu, A. Badmaev and C. Zhou, *Nano Lett.,* 2009 **9**, 3592.

11 Y. Nie, L. Zhang, D. Wu, Y. Chen, G. Zhang, Q. Xie and Z. Liu, *Small*, 2013, **9***,* 1336.

12 Y. Su, S. Pei, J. Du, W.-B. Liu, C. Liu and H.-M. Cheng, *Carbon*, 2013, **53**, 4.

13 T. Sheps, J. Brocious, B. L. Corso, O. T. Gül, D. Whitmore, G. Durkaya, E. O. Potma and P. G. Collins, *Phys. Rev. B*, 2012, **86**, 235412.

14 P. Myllyperkiö, O. Herranen, J. Rintala, H. Jiang, P. R. Mudimela, Z. Zhu, A. G. Nasibulin, A. Johansson, E. I. Kauppinen, M. Ahlskog and M. Pettersson, *ACS Nano*, 2010, **4**, 6780.

15 H. Su, J. Ye, Z. Tang and K. Wong, *Phys. Rev.* B, 2008, **77**, 125428.

16 T. Pedersen and K. Pedersen, *Phys. Rev.* B, 2009, **79,** 035422.

17 M. J. Huttunen, O. Herranen, A. Johansson, H. Jiang, P. R. Mudimela, P. Myllyperkiö, G. Bautista, A. G. Nasibulin, E. I. Kauppinen, M. Ahlskog, M. Kauranen and M. Pettersson, *New J. Phys.,* 2013, **15**, 083043.

18 C. Georgi, N. Hartmann, T. Gokus, A. A. Green, M. C. Hersam and A. Hartschuh, *ChemPhysChem*., 2008, **9**, 1460.

19 H. Harutyunyan, T. Gokus, A. A. Green, M. C. Hersam, M. Allegrini and A. Hartschuh, *Nano Lett.,* 2009, **9**, 2010.

20 K. Yoshikawa, K. Matsuda and Y. Kanemitsu, *J. Phys. Chem. C,* 2010, **114**, 4353.

21 P. Finnie and J. Lefebvre, *ACS Nano,* 2012, **6**, 1702.

22 L. X. Zheng, M. J. O'Connell, S. K. Doorn, X. Z. Liao, Y. H. Zhao, E. A. Akhadov, M. A. Hoffbauer, B. J. Roop, Q. X. Jia, R. C. Dye, D. E. Peterson, S. M. Huang, J. Liu and Y. T. Zhu, *Nat. Mater.,* 2004, **3**, 673.

23 X. L. Wei, Y. Liu, Q. Chen and L. M. Peng, *Nanotech.,* 2008, **19**, 355304.

24 A. V. Krasheninnikov and F. Banhart, *Nat. Mater.,* 2007, **6**, 723.

25 H. Kim, T. Sheps, P. G. Collins and E. O. Potma, *Nano Lett.,* 2009**, 9,** 2991.

26 J. Brocius and E. O. Potma, *Mater. Today*, 2013, **16**, 344.

27 C. Bittencourt, C. Navio, A. Nicolay, B. Ruelle, T. Godfroid, R. Snyders, J.-F. Colomer, M. J. Lagos, X. Ke, G. van Tendeloo, I. Suarez-Martinez and C. P. Ewels, *J. Phys. Chem. C,* 2011, **115**, 20412.

28 N. Dementev, S. Osswald, Y. Gogotsib and E. Borguet, *J. Mater. Chem.*, 2009, **19**, 7904.

29 Y. Zhang, H. Son, J. Zhang, J. Kong and Z. Liu, *J. Phys. Chem. C*, 2007, **111**, 1988.

30 Y. Zhang, L. Xie, J. Zhang, Z. Wu and Z. Liu, *J. Phys. Chem. C*, 2007, **111**, 14031.

31 B. Gao, G. V. Hartland and L. Huang, *J. Phys. Chem. Lett.* 2013, **4**, 3050.

32 J. Shiomi and S. Maruyama, *Phys. Rev. B*, 2006, **73**, 205420.

33 M. Grujicica, G. Caoa, A. M. Raob, T. M. Trittb and S. Nayakc, *Appl. Surf. Sci.,* 2003, **214**, 289.

34 U. J. Kim, C. A. Furtado, X. Liu, G. Chen and P. C. Eklund, *J. Am. Chem. Soc.*, 2005, **127**, 15437.

35 A. Tchernatinsky, S. Desai, G. U. Sumanasekra, C. S. Jayanthi, S. Y. Wu, B. Nagabhirava and B. Alphenaar, *J. Appl. Phys.,* 2006, **99**, 034306.

36 Z. X. Guo, J. W. Ding, Y. Xiao and D. Y. Xing, *Nanotech.,* 2007, **18***,* 465706.

37 M. S. Strano, C. A. Dyke, M. L. Usrey, P. W. Barone, M. J. Allen, H. Shan, C. Kittrell, R. H. Hauge, J. M. Tour and R. E. Smalley, *Science*, 2003, **301**, 1519.

Table of contents

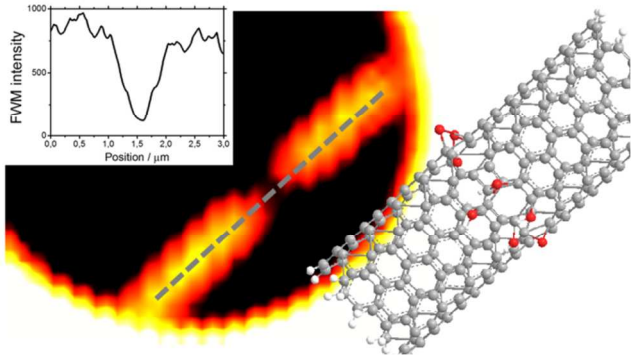

Non-linear photo-oxidation of single walled carbon nanotubes (SWCNT) is induced by femtosecond laser pulses and imaged by four wave mixing microscopy. Oxidation is localized on an individual SWCNT within optical resolution.